

Analysis of accuracy of a finite volume scheme for diffusion equations on distorted meshes [☆]

Guangwei Yuan, Zhiqiang Sheng ^{*}

Laboratory of Computational Physics, Institute of Applied Physics and Computational Mathematics, P.O. Box 8009, Beijing 100088, China

Received 6 August 2006; received in revised form 25 October 2006; accepted 13 November 2006

Available online 2 January 2007

Abstract

We investigate the convergence of a finite volume scheme for the approximation of diffusion operators on distorted meshes. The method was originally introduced by Hermeline [F. Hermeline, A finite volume method for the approximation of diffusion operators on distorted meshes, *J. Comput. Phys.* 160 (2000) 481–499], which has the advantage that highly distorted meshes can be used without the numerical results being altered. In this work, we prove that this method is of first-order accuracy on highly distorted meshes. The results are further extended to the diffusion problems with discontinuous coefficient and non-stationary diffusion problems. Numerical experiments are carried out to confirm the theoretical predications.

© 2006 Elsevier Inc. All rights reserved.

MSC: 65M06; 65M12; 65M55

Keywords: Diffusion equations; Finite volume scheme; Distorted mesh; Accuracy

1. Introduction

Investigating the numerical schemes with high accuracy for the diffusion equation on distorted meshes is very important in Lagrangian hydrodynamics and magnetohydrodynamics. The finite volume method is a discretization technique for solving partial differential equations (PDEs), which is obtained by integrating the PDE over a control volume, and it represents in general the conservation of a quantity of interest, such as mass, momentum, or energy. Due to this natural association, the finite volume method is widely used in practical problems.

A finite volume scheme solving diffusion equation on non-rectangular meshes is introduced in [6], which is the so-called nine point scheme on arbitrary quadrangles. In [2] and [4] a similar scheme for the stationary

[☆] The project is supported by the Special Funds for Major State Basic Research Projects 2005CB321703, the National Nature Science Foundation of China (No. 10476002, 60533020).

^{*} Corresponding author.

E-mail addresses: yuan_guangwei@iapcm.ac.cn (G. Yuan), szqdx@163.com (Z. Sheng).

diffusion equation with smooth coefficient is proposed, but the method of constructing the scheme is different. Moreover, in [2] the unknowns are defined at both the cell-center and the cell-node of primary mesh, and the dual mesh is formed by connecting the center of neighboring primary mesh. Although [2] does not give the theoretical proof, numerical experiments show that this scheme has indeed second accuracy and the numerical solution is independent of the mesh regularity, which demonstrates that the scheme is efficient in solving diffusion equation on Lagrangian meshes.

There are many papers concerning the other numerical schemes for the diffusion equation on distorted meshes, e.g. [1,5,9–18]. The support-operators method (SOM) in [9–14] generally has both cell-center and face-center unknowns or has a dense diffusion matrix, and often leads to a symmetric and positive definite coefficient matrix. However, it does not offer an explicit discrete flux expression. The method of multipoint flux approximations (MPFA) [15,16] whose discrete flux defined on the sub-edge, obtains the explicit discrete flux expression by solving a small scale linear system and often leads to a non-symmetric coefficient matrix for general quadrilateral. The paper [17] presents the relationships among some locally conservative discretization methods.

An interesting application of solving diffusion problems on distorted meshes is the numerical adaptive grid generation (see, e.g. [3,7,8,19]), which is a common tool for use in the numerical solution of partial differential equations on arbitrarily shaped regions. In particular, the meshes are often irregular for solving adaptive moving mesh equations, when the physical governing equations describe certain physical process that undergoes a motion or change with large amplitude.

This paper continues to theoretically analyze the scheme presented in [2], and gives the construction of the scheme for the diffusion equations with discontinuous coefficient. Based on a different approach of devising the finite volume scheme from those in [4–6], we will show the convergence theorem for the finite volume scheme. Specially, we show that the scheme is first-order convergence. Moreover, the theoretical analysis is extended to non-stationary diffusion problem, and the corresponding convergence theorem is obtained. Numerical experiments will verify the theoretical results.

The rest of the paper is organized as follows. In Section 2, we describe the construction of the finite volume scheme on distorted meshes, and state the convergence theorem. In Section 3, the convergence of the scheme is proved, and in Section 4 the scheme for the diffusion equation with discontinuous coefficient is constructed. Moreover the corresponding results for the non-stationary diffusion equation are given in Section 5. Then some numerical examples are presented to show its performance on several test problems in Section 6. Finally, in Section 7 we end with some concluding remarks.

2. Construction of finite volume scheme

Consider the following stationary diffusion problem:

$$-\nabla \cdot (\kappa \nabla u) = f \quad \text{in } \Omega, \quad (1)$$

$$(\kappa \nabla u) \cdot \nu + \lambda u = g \quad \text{on } \partial\Omega, \quad (2)$$

where Ω is an open bounded polygonal set of R^2 with boundary $\partial\Omega$.

Suppose the following conditions (H1) are fulfilled:

(i) There are positive constants $\kappa_1, \kappa_2, \lambda_1, \lambda_2$ such that

$$\kappa_1 \leq \kappa = \kappa(x) \leq \kappa_2, \quad \lambda_1 \leq \lambda = \lambda(x) \leq \lambda_2, \quad \forall x \in \bar{\Omega}.$$

(ii) $\kappa = \kappa(x), \lambda = \lambda(x), f = f(x), g = g(x)$ are continuous functions on $\bar{\Omega}$.

(iii) The problem (1), (2) has a unique solution $u = u(x) \in C^2(\bar{\Omega})$.

We use a mesh on Ω (called primary mesh) made up of arbitrary polygons. With each (primary) element of this mesh we associate one (primary) point: the centroid is a qualified candidate but other points can be chosen. Similarly, with each boundary side we associate one primary point: the midpoint of the boundary side is the natural candidate. Thus we obtain a set of (primary) points that we connect in order to define a second mesh (called dual mesh: see Fig. 1).

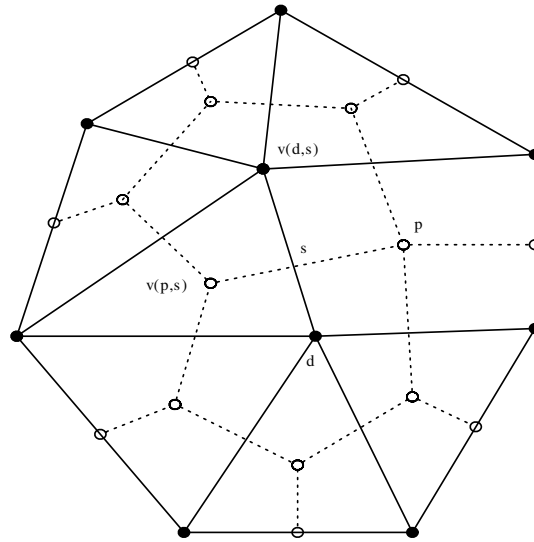


Fig. 1. A sample primary mesh (solid lines) and its dual mesh (dashed lines).

Define the nodes of the primary mesh to be dual points, which will be numbered by d . The primary points are the nodes of dual mesh, which will be numbered by p . Furthermore let us denote by (see Fig. 2)

- v the unit outward normal vector and τ the unit counterclockwise tangent vector on $\partial\Omega$;
- N_P the number of primary points, N_D the number of dual points, N_S the number of sides;
- P_P the primary polygon associated with the primary interior point p ;
- D_d the dual polygon associated with the dual point d ;
- S_{ps} the primary polygon side number s ;
- S_{ds} the dual polygon side number s (not lie on $\partial\Omega$);
- v_{ps} and v_{ds} the unit outward normal vector on the sides S_{ps} and S_{ds} of P_P and D_d ;
- τ_{ps} and τ_{ds} the unit counterclockwise tangent vector on the sides S_{ps} and S_{ds} of P_P and D_d ;

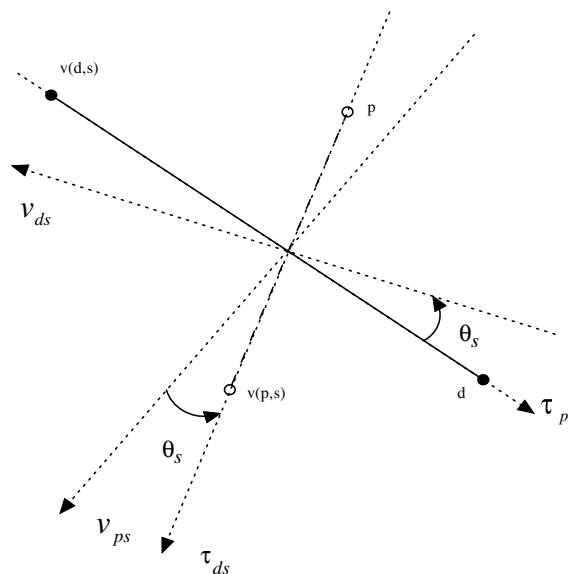


Fig. 2. The primary polygon side $S_{ps} = [d, v(d, s)]$ (solid lines) and the dual polygon side $S_{ds} = [p, v(p, s)]$ (dashed lines).

- $\|P_p\|$ the area of P_p , $\|D_d\|$ the area of D_d and $|S_{ps}|$ the length of the side S_{ps} and $|S_{ds}|$ the length of the side S_{ds} ;
- θ_s the angle between v_{ps} and τ_{ds} ;
- $v(p, s)$ the primary point connected to p by the dual side S_{ds} ;
- $v(d, s)$ the dual point connected to d by the primary side S_{ps} .

Let \mathcal{E} be the sets of all the primary mesh sides, i.e., $\mathcal{E} = \{s : s \in \partial P_p, p \text{ is a primary point}\}$. Let $\mathcal{E}_{\text{int}} = \{s \in \mathcal{E} : s \subset \Omega\}$ be the sets of all the primary mesh sides not on $\partial\Omega$, $\mathcal{E}_{\text{ext}} = \{s \in \mathcal{E} : s \subset \partial\Omega\}$ be the sets of all the primary mesh sides on $\partial\Omega$. Denote $\mathcal{E}' = \{s : s \in \partial D_d \setminus \partial\Omega, d \text{ is a dual point}\}$.

We need the following assumption (H2): There is a constant $C > 0$ such that

$$\frac{1}{C} |S_{ps}| \leq |S_{ds}| \leq C |S_{ps}|, \quad \forall p, \forall d, \forall s,$$

where S_{ps} is the primary polygon side, i.e., the common edge of two neighboring primary cells, and S_{ds} is the dual polygon side, i.e., the line segment connecting the primary cell centroids. Assumption (H2) implicates that the aspect ratio is bounded, i.e., there contain no extremely long, thin cells. The meshes satisfying the assumption (H2) can be found in Figs. 5–10.

In order to construct the finite volume scheme of problem (1), (2), we make the following operations:

- integrate Eq. (1) over each primary polygon P_p ;
- integrate Eq. (2) over each boundary primary side S_{ps} ;
- integrate Eq. (1) over each dual polygon D_d .

Then we obtain

$$-\sum_{s \in \partial P_p} \int_{S_{ps}} \kappa \nabla u \cdot v_{ps} = \int \int_{P_p} f \quad (p \in \Omega), \tag{3}$$

$$\int_{S_{ps} \cap \partial\Omega} \kappa \nabla u \cdot v_{ps} + \int_{S_{ps} \cap \partial\Omega} \lambda u = \int_{S_{ps} \cap \partial\Omega} g \quad (p \in \partial\Omega), \tag{4}$$

$$-\sum_{s \in \partial D_d \setminus \partial\Omega} \int_{S_{ds}} \kappa \nabla u \cdot v_{ds} + \int_{D_d \cap \partial\Omega} \lambda u = \int \int_{D_d} f + \int_{D_d \cap \partial\Omega} g. \tag{5}$$

Denote

$$\mathbf{F}_{ps} = - \int_{S_{ps}} \kappa \nabla u \cdot v_{ps} \quad (p \in \Omega),$$

$$\mathbf{F}_{ds} = - \int_{S_{ds}} \kappa \nabla u \cdot v_{ds} \quad (s \in \partial D_d \setminus \partial\Omega),$$

$$\mathbf{F}_{ps, \partial\Omega} = \int_{S_{ps} \cap \partial\Omega} \kappa \nabla u \cdot v_{ps} \quad (p \in \partial\Omega).$$

Noticing that

$$v_{ps} = -\tan \theta_s \tau_{ps} + \frac{1}{\cos \theta_s} \tau_{ds}, \quad v_{ds} = -\frac{1}{\cos \theta_s} \tau_{ps} + \tan \theta_s \tau_{ds},$$

we obtain

$$\mathbf{F}_{ps} = \tan \theta_s \int_{S_{ps}} \kappa \nabla u \cdot \tau_{ps} - \frac{1}{\cos \theta_s} \int_{S_{ps}} \kappa \nabla u \cdot \tau_{ds} \quad (p \in \Omega),$$

$$\mathbf{F}_{ps, \partial\Omega} = -\tan \theta_s \int_{S_{ps} \cap \partial\Omega} \kappa \nabla u \cdot \tau_{ps} + \frac{1}{\cos \theta_s} \int_{S_{ps} \cap \partial\Omega} \kappa \nabla u \cdot \tau_{ds} \quad (p \in \partial\Omega),$$

$$\mathbf{F}_{ds} = \frac{1}{\cos \theta_s} \int_{S_{ds}} \kappa \nabla u \cdot \tau_{ps} - \tan \theta_s \int_{S_{ds}} \kappa \nabla u \cdot \tau_{ds} \quad (s \in \partial D_d \setminus \partial\Omega).$$

In order to discretize the above continuous fluxes, we use the Taylor expansion for the function $u(x)$, and then obtain

$$u(d) - u(v(d, s)) = \nabla u(x) \cdot (d - v(d, s)) + \int_0^1 (H_d - H_{v(d,s)})r dr,$$

where $H_d = (\nabla^2 u(rx + (1 - r)d)(d - x), d - x)$, $\nabla^2 u(rx + (1 - r)d)$ expresses the Hessian matrix of u at the point $rx + (1 - r)d$. The notation $H_{v(d,s)}$ and the following notations $H_p, H_{v(p,s)}$ have the similar meaning.

Let $\bar{\kappa}_{ps}$ and $\bar{\kappa}_{ds}$ be an average value of κ along the side S_{ps} and S_{ds} , respectively. Then there are

$$\bar{\kappa}_{ps}(u(d) - u(v(d, s))) = \int_{S_{ps}} \kappa \nabla u \cdot \tau_{ps} + \frac{1}{|S_{ps}|} \int_{S_{ps}} \kappa \left(\int_0^1 (H_d - H_{v(d,s)})r dr \right), \tag{6}$$

$$\bar{\kappa}_{ds}(u(v(p, s)) - u(p)) = \int_{S_{ds}} \kappa \nabla u \cdot \tau_{ds} + \frac{1}{|S_{ds}|} \int_{S_{ds}} \kappa \left(\int_0^1 (H_{v(p,s)} - H_p)r dr \right), \tag{7}$$

$$\bar{\kappa}_{ds}(u(d) - u(v(d, s))) = \frac{|S_{ps}|}{|S_{ds}|} \int_{S_{ds}} \kappa \nabla u \cdot \tau_{ps} + \frac{1}{|S_{ds}|} \int_{S_{ds}} \kappa \left(\int_0^1 (H_d - H_{v(d,s)})r dr \right), \tag{8}$$

$$\bar{\kappa}_{ps}(u(v(p, s)) - u(p)) = \frac{|S_{ds}|}{|S_{ps}|} \int_{S_{ps}} \kappa \nabla u \cdot \tau_{ds} + \frac{1}{|S_{ps}|} \int_{S_{ps}} \kappa \left(\int_0^1 (H_{v(p,s)} - H_p)r dr \right). \tag{9}$$

The second terms of right hand in the above four equations are $O(h^2)$. Denote

$$\bar{F}_{ps} = \tan \theta_s \bar{\kappa}_{ps}(u(d) - u(v(d, s))) - \frac{\bar{\kappa}_{ps}}{\cos \theta_s} \frac{|S_{ps}|}{|S_{ds}|} (u(v(p, s)) - u(p)) \quad (p \in \Omega), \tag{10}$$

$$\bar{F}_{ps, \partial\Omega} = -\frac{\bar{\kappa}_{ps}}{\cos \theta_s} \frac{|S_{ps}|}{|S_{ds}|} (u(v(p, s)) - u(p)) + \tan \theta_s \bar{\kappa}_{ps}(u(d) - u(v(d, s))) \quad (p \in \partial\Omega), \tag{11}$$

$$\bar{F}_{ds} = \frac{\bar{\kappa}_{ds}}{\cos \theta_s} \frac{|S_{ds}|}{|S_{ps}|} (u(d) - u(v(d, s))) - \tan \theta_s \bar{\kappa}_{ds}(u(v(p, s)) - u(p)) \quad (s \in \partial D_d \setminus \partial\Omega). \tag{12}$$

Then, using Eqs. (6)–(9) and the assumption **(H2)**, we have

$$\mathbf{F}_{ps} = \bar{F}_{ps} + R_{ps}|S_{ps}|, \quad \mathbf{F}_{ps, \partial\Omega} = \bar{F}_{ps, \partial\Omega} + R_{ps, \partial\Omega}|S_{ps} \cap \partial\Omega|, \quad \mathbf{F}_{ds} = \bar{F}_{ds} + R_{ds}|S_{ds}|, \tag{13}$$

where $R_{ps}|S_{ps}| = O(h^2)$, $R_{ps, \partial\Omega}|S_{ps} \cap \partial\Omega| = O(h^2)$, $R_{ds}|S_{ds}| = O(h^2)$ and $R_{ps} = -R_{v(p,s)s}$, $R_{ds} = -R_{v(d,s)s}$.

Eqs. (10)–(12) can be rewritten to

$$\bar{F}_{ps} = -\frac{\bar{\kappa}_{ps}}{\cos \theta_s} \frac{|S_{ps}|}{|S_{ds}|} \left(u(v(p, s)) - u(p) - \frac{|S_{ds}|}{|S_{ps}|} \sin \theta_s (u(d) - u(v(d, s))) \right) \quad (p \in \Omega),$$

$$\bar{F}_{ps, \partial\Omega} = -\frac{\bar{\kappa}_{ps}}{\cos \theta_s} \frac{|S_{ps}|}{|S_{ds}|} \left(u(v(p, s)) - u(p) - \frac{|S_{ds}|}{|S_{ps}|} \sin \theta_s (u(d) - u(v(d, s))) \right) \quad (p \in \partial\Omega),$$

$$\bar{F}_{ds} = -\frac{\bar{\kappa}_{ds}}{\cos \theta_s} \frac{|S_{ds}|}{|S_{ps}|} \left(u(v(d, s)) - u(d) - \frac{|S_{ps}|}{|S_{ds}|} \sin \theta_s (u(p) - u(v(p, s))) \right) \quad (s \in \partial D_d \setminus \partial\Omega).$$

Denote

$$f_p = \frac{1}{\|P_p\|} \int \int_{P_p} f, \quad f_d = \frac{1}{\|D_d\|} \int \int_{D_d} f, \quad g_d = \frac{1}{|D_d \cap \partial\Omega|} \int_{D_d \cap \partial\Omega} g,$$

$$g_p = \frac{1}{|S_{ps} \cap \partial\Omega|} \int_{S_{ps} \cap \partial\Omega} g, \quad \lambda_p = \frac{1}{|S_{ps} \cap \partial\Omega|} \int_{S_{ps} \cap \partial\Omega} \lambda.$$

The finite volume scheme of the problem (1), (2) is defined as follows:

$$\sum_{s \in \partial P_p} F_{ps} = \|P_p\| f_p, \quad p \in \Omega, \tag{14}$$

$$F_{ps, \partial\Omega} + |S_{ps} \cap \partial\Omega| \lambda_p u_p = |S_{ps} \cap \partial\Omega| g_p, \quad p \in \partial\Omega, \tag{15}$$

$$\sum_{s \in \partial D_d \setminus \partial\Omega} F_{ds} + |D_d \cap \partial\Omega| \lambda_d u_d = \|D_d\| f_d + |D_d \cap \partial\Omega| g_d, \tag{16}$$

where u_p, u_d are the unknown discrete functions, and

$$F_{ps} = -\frac{\bar{\kappa}_{ps}}{\cos \theta_s} \frac{|S_{ps}|}{|S_{ds}|} \left(u_{v(p,s)} - u_p - \frac{|S_{ds}|}{|S_{ps}|} \sin \theta_s (u_d - u_{v(d,s)}) \right) \quad (p \in \Omega), \tag{17}$$

$$F_{ps,\partial\Omega} = -\frac{\bar{\kappa}_{ps}}{\cos \theta_s} \frac{|S_{ps}|}{|S_{ds}|} \left(u_{v(p,s)} - u_p - \frac{|S_{ds}|}{|S_{ps}|} \sin \theta_s (u_d - u_{v(d,s)}) \right) \quad (p \in \partial\Omega), \tag{18}$$

$$F_{ds} = -\frac{\bar{\kappa}_{ds}}{\cos \theta_s} \frac{|S_{ds}|}{|S_{ps}|} \left(u_{v(d,s)} - u_d - \frac{|S_{ps}|}{|S_{ds}|} \sin \theta_s (u_p - u_{v(p,s)}) \right) \quad (s \in \partial D_d \setminus \partial\Omega). \tag{19}$$

Introduce the following assumption **(H3)**: There is a constant $\varepsilon \in (0, 1)$, such that

$$[4\bar{\kappa}_{ps}\bar{\kappa}_{ds} - (\bar{\kappa}_{ps} + \bar{\kappa}_{ds})^2 \sin^2 \theta_s] \min \left(\frac{|S_{ds}|}{\bar{\kappa}_{ps}|S_{ps}|}, \frac{|S_{ps}|}{\bar{\kappa}_{ds}|S_{ds}|} \right) \geq \varepsilon.$$

Let $\psi = 4\bar{\kappa}_{ps}\bar{\kappa}_{ds} - (\bar{\kappa}_{ps} + \bar{\kappa}_{ds})^2 \sin^2 \theta_s$. The assumption **(H3)** requires $\psi > 0$. From the definition of θ_s , θ_s describes the degree of mesh distorted, and there is $0 \leq \theta_s < \frac{\pi}{2}$. Hence, the assumption **(H3)** implies a geometric constraint on the cell deformation. For a orthogonal mesh, there hold $\theta_s = 0$, so that $\psi > 0$. When $\bar{\kappa}_{ps} = \bar{\kappa}_{ds} = \bar{\kappa}_s$, it is obvious that $\psi = 4\bar{\kappa}_s^2(1 - \sin^2 \theta_s) > 0$. Therefore, the assumption **(H3)** can be easily satisfied.

Denote $e_p = u(p) - u_p$, $e_d, e_{v(p,s)}, e_{v(d,s)}$ have the similar definitions. For $s \in \mathcal{E}$, define $\nabla_s e = |e_p - e_{v(p,s)}|$; for $s \in \mathcal{E}'$, define $\nabla_s e = |e_d - e_{v(d,s)}|$. Define $\|\nabla e\|_2^2 = \sum_{s \in \mathcal{E}} (\nabla_s e)^2$, $\|\bar{\nabla} e\|_2^2 = \sum_{s \in \mathcal{E}'} (\nabla_s e)^2$.

Then we will obtain the following theorem:

Theorem 1. Assume **(H1)**–**(H3)** are satisfied. Then there are

$$\|\nabla e\|_2 + \|\bar{\nabla} e\|_2 \leq Ch,$$

where C is a positive constant dependent only on the known data and ε .

Remark 1. There is an one-one mapping between \mathcal{E} and \mathcal{E}' : if $s \in \mathcal{E}$ and s is a segment connecting p with $v(p,s)$, then it is corresponding to $s \in \mathcal{E}'$ which is a segment connecting $v(d,s)$ with d . Thus, in the following the notation $\sum_{s \in \mathcal{E}'}$ will be replaced by $\sum_{s \in \mathcal{E}}$.

Remark 2. Let the matrix of linear system resulting from the finite volume scheme (14)–(16) be A . If for all s , $\bar{\kappa}_{ps} = \bar{\kappa}_{ds}$, then A is symmetric positive definite. If there exists s such that $\bar{\kappa}_{ps} \neq \bar{\kappa}_{ds}$, then A is no more symmetric but it remains positive definite if the assumption **(H3)** holds (see [2]).

3. Proof of Theorem 1

Using Eqs. (3)–(5), we get

$$\sum_{s \in \partial P_p} \mathbf{F}_{ps} = \|P_p\| f_p \quad (p \in \Omega),$$

$$\mathbf{F}_{ps,\partial\Omega} + \int_{S_{ps} \cap \partial\Omega} \lambda u = |S_{ps} \cap \partial\Omega| g_p \quad (p \in \partial\Omega),$$

$$\sum_{s \in \partial D_d \setminus \partial\Omega} \mathbf{F}_{ds} + \int_{D_d \cap \partial\Omega} \lambda u = \|D_d\| f_d + |D_d \cap \partial\Omega| g_d.$$

Hence there are

$$\sum_{s \in \partial P_p} \bar{F}_{ps} = - \sum_{s \in \partial P_p} R_{ps} |S_{ps}| + \|P_p\| f_p \quad (p \in \Omega), \tag{20}$$

$$\bar{F}_{ps,\partial\Omega} + |S_{ps} \cap \partial\Omega| \lambda_p u(p) = \int_{S_{ps} \cap \partial\Omega} \lambda(x) (u(p) - u(x)) + |S_{ps} \cap \partial\Omega| (g_p - R_{ps,\partial\Omega}) \quad (p \in \partial\Omega), \tag{21}$$

$$\sum_{s \in \partial D_d \setminus \partial \Omega} \bar{F}_{ds} + |D_d \cap \partial \Omega| \lambda_d u(d) = - \sum_{s \in \partial D_d \setminus \partial \Omega} R_{ds} |S_{ds}| + \int_{D_d \cap \partial \Omega} \lambda(x)(u(d) - u(x)) + \|D_d\| f_d + |D_d \cap \partial \Omega| g_d. \tag{22}$$

Denote

$$G_{ps} = \bar{F}_{ps} - F_{ps}, \quad G_{ds} = \bar{F}_{ds} - F_{ds}, \quad G_{ps, \partial \Omega} = \bar{F}_{ps, \partial \Omega} - F_{ps, \partial \Omega}.$$

Then, by using of Eqs. (14)–(16) and (20)–(22), there are

$$\sum_{s \in \partial P_p} G_{ps} = - \sum_{s \in \partial P_p} R_{ps} |S_{ps}| \quad (p \in \Omega), \tag{23}$$

$$G_{ps, \partial \Omega} + |S_{ps} \cap \partial \Omega| \lambda_p e_p = \int_{S_{ps} \cap \partial \Omega} \lambda(x)(u(p) - u(x)) - R_{ps, \partial \Omega} |S_{ps} \cap \partial \Omega| \quad (p \in \partial \Omega), \tag{24}$$

$$\sum_{s \in \partial D_d \setminus \partial \Omega} G_{ds} + |D_d \cap \partial \Omega| \lambda_d e_d = - \sum_{s \in \partial D_d \setminus \partial \Omega} R_{ds} |S_{ds}| + \int_{D_d \cap \partial \Omega} \lambda(x)(u(d) - u(x)), \tag{25}$$

where

$$G_{ps} = - \frac{\bar{\kappa}_{ps}}{\cos \theta_s} \frac{|S_{ps}|}{|S_{ds}|} \left(e_{v(p,s)} - e_p - \frac{|S_{ds}|}{|S_{ps}|} \sin \theta_s (e_d - e_{v(d,s)}) \right) \quad (p \in \Omega),$$

$$G_{ps, \partial \Omega} = - \frac{\bar{\kappa}_{ps}}{\cos \theta_s} \frac{|S_{ps} \cap \partial \Omega|}{|S_{ds}|} \left(e_{v(p,s)} - e_p - \frac{|S_{ds}|}{|S_{ps} \cap \partial \Omega|} \sin \theta_s (e_d - e_{v(d,s)}) \right) \quad (p \in \partial \Omega),$$

$$G_{ds} = - \frac{\bar{\kappa}_{ds}}{\cos \theta_s} \frac{|S_{ds}|}{|S_{ps}|} \left(e_{v(d,s)} - e_d - \frac{|S_{ps}|}{|S_{ds}|} \sin \theta_s (e_p - e_{v(p,s)}) \right) \quad (s \in \partial D_d \setminus \partial \Omega).$$

Making the scalar product of e_p with Eqs. (23), (24) and e_d with (25), and summing up the resulting products for $p \in \Omega$, $p \in \partial \Omega$ and d , we get

$$\begin{aligned} & \sum_{p \in \Omega} \sum_{s \in \partial P_p} G_{ps} e_p + \sum_{p \in \partial \Omega} G_{ps, \partial \Omega} e_p + \sum_{p \in \partial \Omega} \lambda_p e_p^2 |S_{ps} \cap \partial \Omega| + \sum_d \sum_{s \in \partial D_d \setminus \partial \Omega} G_{ds} e_d + \sum_{d \in \partial \Omega} \lambda_d e_d^2 |D_d \cap \partial \Omega| \\ &= - \sum_{p \in \Omega} \sum_{s \in \partial P_p} R_{ps} e_p |S_{ps}| - \sum_d \sum_{s \in \partial D_d \setminus \partial \Omega} R_{ds} e_d |S_{ds}| - \sum_{p \in \partial \Omega} R_{ps, \partial \Omega} |S_{ps} \cap \partial \Omega| e_p + \sum_{p \in \partial \Omega} e_p \int_{S_{ps} \cap \partial \Omega} \lambda(x)(u(p) - u(x)) \\ & \quad + \sum_{d \in \partial \Omega} e_d \int_{D_d \cap \partial \Omega} \lambda(x)(u(d) - u(x)). \end{aligned} \tag{26}$$

Noticing that $R_{ps} = -R_{v(p,s)s}$ and $R_{ds} = -R_{v(d,s)s}$, we denote $R_s = |R_{ps}|$ and $\bar{R}_s = |R_{ds}|$. In the former section, we have proved that $R_s |S_{ps}| = O(h^2)$ and $\bar{R}_s |S_{ds}| = O(h^2)$. Then it follows that

$$\begin{aligned} \left| \sum_{p \in \Omega} \sum_{s \in \partial P_p} R_{ps} e_p |S_{ps}| + \sum_{p \in \partial \Omega} R_{ps, \partial \Omega} |S_{ps} \cap \partial \Omega| e_p \right| &\leq \sum_{s \in \mathcal{E}} |R_{ps}| R_s \nabla_s e \leq \left(\sum_{s \in \mathcal{E}} (\nabla_s e)^2 \right)^{\frac{1}{2}} \left(\sum_{s \in \mathcal{E}} (|S_{ps}| R_s)^2 \right)^{\frac{1}{2}} \\ &\leq Ch \|\nabla e\|_2 \leq \frac{\varepsilon}{16} \|\nabla e\|_2^2 + \frac{C}{\varepsilon} h^2, \end{aligned} \tag{27}$$

$$\begin{aligned} \left| \sum_d \sum_{s \in \partial D_d \setminus \partial \Omega} R_{ds} e_d |S_{ds}| \right| &\leq \sum_{s \in \mathcal{E}_{\text{int}}} |S_{ds}| \bar{R}_s \bar{\nabla}_s e \leq \left(\sum_{s \in \mathcal{E}_{\text{int}}} (\bar{\nabla}_s e)^2 \right)^{\frac{1}{2}} \left(\sum_{s \in \mathcal{E}_{\text{int}}} (|S_{ds}| \bar{R}_s)^2 \right)^{\frac{1}{2}} \leq Ch \|\bar{\nabla} e\|_2 \\ &\leq \frac{\varepsilon}{16} \|\bar{\nabla} e\|_2^2 + \frac{C}{\varepsilon} h^2. \end{aligned} \tag{28}$$

Obviously, there are

$$\begin{aligned} \left| \sum_{p \in \partial\Omega} e_p \int_{S_{ps} \cap \partial\Omega} \lambda(x)(u(p) - u(x)) \right| &\leq Ch \sum_{p \in \partial\Omega} \lambda_p |e_p| |S_{ps} \cap \partial\Omega| \\ &\leq \frac{1}{4} \sum_{p \in \partial\Omega} \lambda_p e_p^2 |S_{ps} \cap \partial\Omega| + Ch^2 \sum_{p \in \partial\Omega} \lambda_p |S_{ps} \cap \partial\Omega|, \end{aligned} \tag{29}$$

$$\begin{aligned} \left| \sum_{d \in \partial\Omega} e_d \int_{D_d \cap \partial\Omega} \lambda(x)(u(d) - u(x)) \right| &\leq Ch \sum_{d \in \partial\Omega} \lambda_d |e_d| |D_d \cap \partial\Omega| \\ &\leq \frac{1}{2} \sum_{d \in \partial\Omega} \lambda_d e_d^2 |D_d \cap \partial\Omega| + Ch^2 \sum_{d \in \partial\Omega} \lambda_d |D_d \cap \partial\Omega|. \end{aligned} \tag{30}$$

Combining (26)–(30), we get

$$\begin{aligned} &\sum_{s \in \mathcal{E}} \frac{1}{\cos \theta_s} \left(\bar{\kappa}_{ps} \frac{|S_{ps}|}{|S_{ds}|} (e_p - e_{v(p,s)})^2 + \bar{\kappa}_{ds} \frac{|S_{ds}|}{|S_{ps}|} (e_d - e_{v(d,s)})^2 + (\bar{\kappa}_{ps} + \bar{\kappa}_{ds}) \sin \theta_s (e_p - e_{v(p,s)})(e_d - e_{v(d,s)}) \right) \\ &\quad + \frac{1}{2} \sum_{p \in \partial\Omega} \lambda_p e_p^2 |S_{ps} \cap \partial\Omega| + \frac{1}{2} \sum_{d \in \partial\Omega} \lambda_d e_d^2 |D_d \cap \partial\Omega| \\ &\leq Ch^2 + \frac{\varepsilon}{16} (\|\nabla e\|_2^2 + \|\bar{\nabla} e\|_2^2), \end{aligned} \tag{31}$$

where $C = C(\varepsilon)$ is a positive constant dependent only on the known data and ε . Notice that there holds the following inequality: for $a > 0, c > 0$, there are

$$ax^2 + bxy + cy^2 \geq \frac{4ac - b^2}{8} \min\left(\frac{1}{a}, \frac{1}{c}\right) (x^2 + y^2).$$

Hence, from the assumption **(H3)** and (31), it follows

$$\|\nabla e\|_2^2 + \|\bar{\nabla} e\|_2^2 + \sum_{p \in \partial\Omega} \lambda_p e_p^2 |S_{ps} \cap \partial\Omega| + \sum_{d \in \partial\Omega} \lambda_d e_d^2 |D_d \cap \partial\Omega| \leq Ch^2, \tag{32}$$

where $C = C(\varepsilon)$. The proof of Theorem 1 is finished. \square

4. Problems with discontinuous coefficient

In this section, we construct the scheme for the diffusion equations with discontinuous coefficient. Assume that the primary elements are homogeneous, but the material properties may vary between primary elements. Hence, the dual elements may contain different materials, and we denote it by $-$ and $+$, respectively (see Fig. 3). For convenience, we introduce some new notations (see Fig. 4) here. Let σ be the dual polygon side $S_{ds} = [p, v(p, s)]$. Let $d_{d,\sigma}$ be the distance between d and σ , and $d_{v(d,s),\sigma}$ be the distance between $v(d, s)$ and σ . I is the point of intersection of the segments $pv(p, s)$ and $dv(d, s)$. Moreover let $\vec{n}_{d,\sigma}$ and $\vec{n}_{v(d,s),\sigma}$ be the unit normal vectors on the edge σ and $\vec{t}_{d,\sigma}$ and $\vec{t}_{v(d,s),\sigma}$ be the unit tangent vectors on the edge σ . Denote σ_+ be the distance between I and $v(p, s)$, and σ_- be the distance between p and I .

Note that $I - d = d_{d,\sigma} \vec{n}_{d,\sigma} - r_+ \vec{t}_{d,\sigma}$, and by the Taylor expansion,

$$u(I) - u(d) = \nabla u(x) \cdot (I - d) + \int_0^1 (H_I - H_d) s ds, \quad x \in \sigma.$$

Then we have

$$\frac{u(I) - u(d)}{d_{d,\sigma}} \int_{S_{ds}} \kappa(x) dl = \int_{S_{ds}} \kappa(x) \nabla u(x) \cdot \vec{n}_{d,\sigma} dl - \frac{r_+}{d_{d,\sigma}} \int_{S_{ds}} \kappa(x) \nabla u(x) \cdot \vec{t}_{d,\sigma} + \int_{S_{ds}} \frac{\kappa(x)}{d_{d,\sigma}} \int_0^1 (H_I - H_d) s ds dl. \tag{33}$$

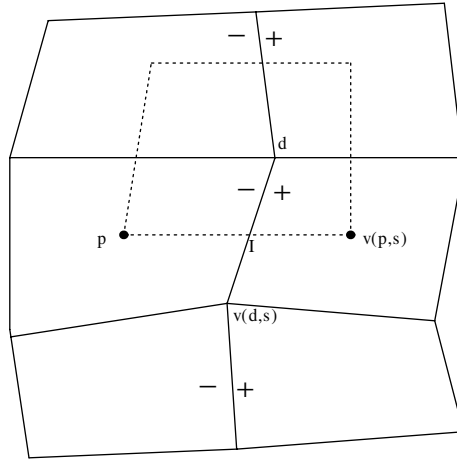


Fig. 3. A sample primary mesh (solid lines) and its dual mesh (dashed lines) with the discontinuous line.

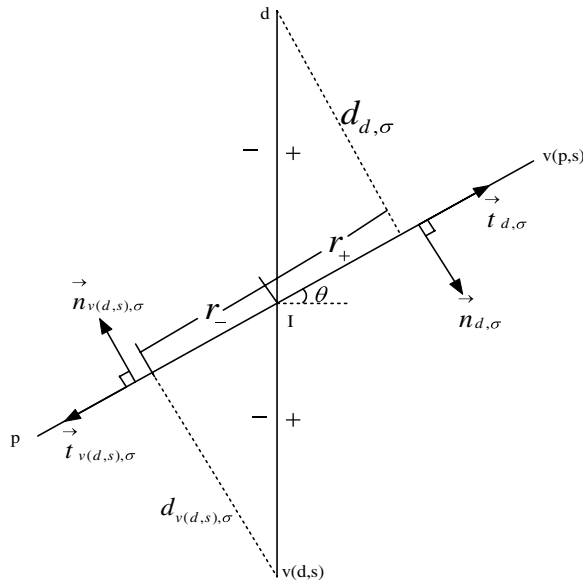


Fig. 4. Notations.

Similarly, there are

$$\begin{aligned} \frac{u(I) - u(v(d,s))}{d_{v(d,s),\sigma}} \int_{S_{ds}} \kappa(x) dl &= \int_{S_{ds}} \kappa(x) \nabla u(x) \cdot \vec{n}_{v(d,s),\sigma} dl - \frac{r_-}{d_{v(d,s),\sigma}} \int_{S_{ds}} \kappa(x) \nabla u(x) \cdot \vec{t}_{v(d,s),\sigma} \\ &+ \int_{S_{ds}} \frac{\kappa(x)}{d_{v(d,s),\sigma}} \int_0^1 (H_I - H_{v(d,s)}) s ds dl. \end{aligned} \tag{34}$$

Denote

$$\tau_{d,\sigma} = \frac{\int_{S_{ds}} \kappa(x) dl}{d_{d,\sigma}}, \quad \tau_{v(d,s),\sigma} = \frac{\int_{S_{ds}} \kappa(x) dl}{d_{v(d,s),\sigma}}.$$

Note that $\vec{n}_{v(d,s),\sigma} = -\vec{n}_{d,\sigma}$ and $\vec{t}_{v(d,s),\sigma} = -\vec{t}_{d,\sigma}$. We have

$$\begin{aligned} \int_{S_{ds}} \kappa(x) \nabla u(x) \cdot \vec{n}_{d,\sigma} \, dl &= \frac{1}{2} \left[\tau_{d,\sigma} (u(I) - u(d)) + \tau_{v(d,s),\sigma} (u(v(d,s)) - u(I)) \right. \\ &\quad \left. + \left(\frac{r_+}{\tau_{d,\sigma}} + \frac{r_-}{\tau_{v(d,s),\sigma}} \right) \int_{S_{ds}} \kappa(x) \nabla u(x) \cdot \vec{t}_{d,\sigma} \, dl \right] \\ &\quad + \frac{1}{2} \left(\frac{1}{d_{v(d,s),\sigma}} \int_{S_{ds}} \kappa(x) \int_0^1 (H_I - H_{v(d,s)}) s \, ds \, dl + \frac{1}{d_{d,\sigma}} \int_{S_{ds}} \kappa(x) \int_0^1 (H_d - H_I) s \, ds \, dl \right). \end{aligned} \tag{35}$$

By the continuity of the normal flux

$$\int_{S_{ds}} \kappa(x) \nabla u(x) \cdot \vec{n}_{v(d,s),\sigma} \, dl = - \int_{S_{ds}} \kappa(x) \nabla u(x) \cdot \vec{n}_{d,\sigma} \, dl$$

and $\frac{r_+}{d_{d,\sigma}} = \frac{r_-}{d_{v(d,s),\sigma}}$, we have

$$u(I) = \frac{\tau_{d,\sigma} u(d) + \tau_{v(d,s),\sigma} u(v(d,s))}{\tau_{d,\sigma} + \tau_{v(d,s),\sigma}} + O(h^2). \tag{36}$$

Similarly, we have

$$\frac{u(v(p,s)) - u(I)}{|v(p,s) - I|} \int_{\sigma_+} \kappa^+(x) \, dl = \int_{\sigma_+} \kappa^+(x) \nabla u^+(x) \cdot \vec{t}_{d,\sigma} \, dl + \frac{1}{|v(p,s) - I|} \int_{\sigma_+} \kappa^+(x) \int_0^1 (H_{v(p,s)} - H_I^+) s \, ds \, dl$$

and

$$\frac{u(I) - u(p)}{|I - p|} \int_{\sigma_-} \kappa^-(x) \, dl = \int_{\sigma_-} \kappa^-(x) \nabla u^-(x) \cdot \vec{t}_{d,\sigma} \, dl + \frac{1}{|I - p|} \int_{\sigma_-} \kappa^-(x) \int_0^1 (H_I^- - H_p) s \, ds \, dl.$$

Combine the above two equations to obtain

$$\begin{aligned} \int_{S_{ds}} \kappa(x) \nabla u(x) \cdot \vec{t}_{d,\sigma} \, dl &= \frac{u(v(p,s)) - u(I)}{|v(p,s) - I|} \int_{\sigma_+} \kappa^+(x) \, dl + \frac{u(I) - u(p)}{|I - p|} \int_{\sigma_-} \kappa^-(x) \, dl - \frac{1}{|v(p,s) - I|} \\ &\quad \times \int_{\sigma_+} \kappa^+(x) \int_0^1 (H_{v(p,s)} - H_I^+) s \, ds \, dl - \frac{1}{|I - p|} \int_{\sigma_-} \kappa^-(x) \int_0^1 (H_I^- - H_p) s \, ds \, dl. \end{aligned} \tag{37}$$

Substitute (36) and (37) into (35) to obtain

$$\begin{aligned} \int_{S_{ds}} \kappa(x) \nabla u(x) \cdot \vec{n}_{d,\sigma} \, dl &= \left[\tau_\sigma + \frac{(d_{d,\sigma} - d_{v(d,s),\sigma})}{4(d_{d,\sigma} + d_{v(d,s),\sigma})} \left(\frac{r_+}{d_{d,\sigma}} + \frac{r_-}{d_{v(d,s),\sigma}} \right) \left(\frac{1}{|\sigma_-|} \int_{\sigma_-} \kappa^-(x) \, dl - \frac{1}{|\sigma_+|} \int_{\sigma_+} \kappa^+(x) \, dl \right) \right] \\ &\quad \times (u(v(d,s)) - u(d)) + \frac{1}{4} \left(\frac{r_+}{d_{d,\sigma}} + \frac{r_-}{d_{v(d,s),\sigma}} \right) \left[\left(\frac{1}{|\sigma_-|} \int_{\sigma_-} \kappa^-(x) \, dl + \frac{1}{|\sigma_+|} \int_{\sigma_+} \kappa^+(x) \, dl \right) \right. \\ &\quad \times (u(v(p,s)) - u(p)) + \left(\frac{1}{|\sigma_-|} \int_{\sigma_-} \kappa^-(x) \, dl - \frac{1}{|\sigma_+|} \int_{\sigma_+} \kappa^+(x) \, dl \right) \\ &\quad \left. \times (u(d) + u(v(d,s)) - u(v(p,s)) - u(p)) \right] + O(h^2), \end{aligned}$$

where

$$\tau_\sigma = \frac{\tau_{d,\sigma} \tau_{v(d,s),\sigma}}{\tau_{d,\sigma} + \tau_{v(d,s),\sigma}} = \frac{\int_{S_{ds}} \kappa(x) \, dl}{\tau_{d,\sigma} + \tau_{v(d,s),\sigma}}.$$

Hence, we define

$$F_{ds} = - \left[\tau_\sigma + \frac{(d_{d,\sigma} - d_{v(d,s),\sigma})}{4(d_{d,\sigma} + d_{v(d,s),\sigma})} \left(\frac{r_+}{d_{d,\sigma}} + \frac{r_-}{d_{v(d,s),\sigma}} \right) \left(\frac{\int_{\sigma_-} \kappa^-(x) dl}{|\sigma_-|} - \frac{\int_{\sigma_+} \kappa^+(x) dl}{|\sigma_+|} \right) \right] (u_{v(d,s)} - u_d) - \frac{1}{4} \left(\frac{r_+}{d_{d,\sigma}} + \frac{r_-}{d_{v(d,s),\sigma}} \right) \left[\frac{\int_{\sigma_-} \kappa^-(x) dl}{|\sigma_-|} (u_d + u_{v(d,s)} - 2u_p) - \frac{\int_{\sigma_+} \kappa^+(x) dl}{|\sigma_+|} (u_d + u_{v(d,s)} - 2u_{v(p,s)}) \right]. \tag{38}$$

When $\kappa(x)$ is continuous across σ , there is $\frac{\int_{\sigma_-} \kappa^-(x) dl}{|\sigma_-|} \approx \frac{\int_{\sigma_+} \kappa^+(x) dl}{|\sigma_+|} \approx \bar{\kappa}_{ds}$. Hence

$$F_{ds} = -\tau_\sigma(u_{v(d,s)} - u_d) - \frac{1}{4} \left(\frac{r_+}{d_{d,\sigma}} + \frac{r_-}{d_{v(d,s),\sigma}} \right) \bar{\kappa}_{ds} (2u_{v(p,s)} - 2u_p) = \frac{\bar{\kappa}_{ds}}{\cos \theta_s} \frac{|S_{ds}|}{|S_{ps}|} (u_d - u_{v(d,s)}) - \tan \theta_s \bar{\kappa}_{ds} (u_{v(p,s)} - u_p),$$

i.e., F_{ds} is reduced to (19).

An analogous derivation for primary elements gives the definition

$$F_{ps} = - \frac{|S_{ps}|}{\cos \theta_s} \frac{\bar{\kappa}^- \bar{\kappa}^+}{\sigma_+ \bar{\kappa}^- + \sigma_- \bar{\kappa}^+} \left(u_{v(p,s)} - u_p - \frac{|S_{ds}|}{|S_{ps}|} \sin \theta_s (u_d - u_{v(d,s)}) \right), \tag{39}$$

where $\bar{\kappa}^- = \frac{\int_{S_{ps}} \kappa^-(x) dl}{|S_{ps}|}$, $\bar{\kappa}^+ = \frac{\int_{S_{ps}} \kappa^+(x) dl}{|S_{ps}|}$. When $\kappa(x)$ is continuous across S_{ps} , there is $\bar{\kappa}^+ = \bar{\kappa}^- = \bar{\kappa}_{ps}$. Hence

$$F_{ps} = - \frac{\bar{\kappa}_{ps}}{\cos \theta_s} \frac{|S_{ps}|}{|S_{ds}|} \left(u_{v(p,s)} - u_p - \frac{|S_{ds}|}{|S_{ps}|} \sin \theta_s (u_d - u_{v(d,s)}) \right),$$

i.e., F_{ps} is reduced to (17).

Hence, we can obtain the finite volume scheme for the diffusion equation with discontinuous coefficient.

5. Non-stationary diffusion problem

In this section, we will extend the previous results to the following diffusion problem:

$$u_t - \nabla \cdot (\kappa(x, t) \nabla u) = f(x, t) \quad \text{in } \Omega \times (0, T], \tag{40}$$

$$(\kappa(x, t) \nabla u) \cdot \nu + \lambda(x, t) u = g(x, t) \quad \text{on } \partial\Omega \times [0, T], \tag{41}$$

$$u(x, 0) = \varphi(x) \quad \text{on } \Omega. \tag{42}$$

The notations have the similar meaning as those in the Section 2. Discretize the time segment by $0 = t^0 < T^1 < \dots < T_{N+1} = T$, $t^n = n\Delta t$. We adopt the implicit scheme for the problem (40)–(42) and the same discretization as the Section 2 for the diffusion term, source term and the initial-boundary condition. We can get the following finite volume scheme:

$$\|P_p\| \frac{u_p^{n+1} - u_p^n}{\Delta t} + \sum_{s \in \partial P_p} F_{ps}^{n+1} = \|P_p\| f_p^{n+1}, \quad p \in \Omega, \tag{43}$$

$$F_{ps, \partial\Omega}^{n+1} + |S_{ps} \cap \partial\Omega| \lambda_p^{n+1} u_p^{n+1} = |S_{ps} \cap \partial\Omega| g_p^{n+1}, \quad p \in \partial\Omega, \tag{44}$$

$$\|D_d\| \frac{u_d^{n+1} - u_d^n}{\Delta t} + \sum_{s \in \partial D_d \cap \partial\Omega} F_{ds}^{n+1} + |D_d \cap \partial\Omega| \lambda_d^{n+1} u_d^{n+1} = \|D_d\| f_d^{n+1} + |D_d \cap \partial\Omega| g_d^{n+1}, \tag{45}$$

where u_p^{n+1} , u_d^{n+1} are the unknown discrete functions defined on the primary mesh and the dual mesh respectively, and

$$\begin{aligned}
 F_{ps}^{n+1} &= -\frac{\bar{\kappa}_{ps}^{n+1}}{\cos \theta_s} \frac{|S_{ps}|}{|S_{ds}|} \left(u_{v(p,s)}^{n+1} - u_p^{n+1} - \frac{|S_{ds}|}{|S_{ps}|} \sin \theta_s (u_d^{n+1} - u_{v(d,s)}^{n+1}) \right) \quad (p \in \Omega), \\
 F_{ps,\partial\Omega}^{n+1} &= -\frac{\bar{\kappa}_{ps}^{n+1}}{\cos \theta_s} \frac{|S_{ps}|}{|S_{ds}|} \left(u_{v(p,s)}^{n+1} - u_p^{n+1} - \frac{|S_{ds}|}{|S_{ps}|} \sin \theta_s (u_d^{n+1} - u_{v(d,s)}^{n+1}) \right) \quad (p \in \partial\Omega), \\
 F_{ds}^{n+1} &= -\frac{\bar{\kappa}_{ds}^{n+1}}{\cos \theta_s} \frac{|S_{ds}|}{|S_{ps}|} \left(u_{v(d,s)}^{n+1} - u_d^{n+1} - \frac{|S_{ps}|}{|S_{ss}|} \sin \theta_s (u_p^{n+1} - u_{v(p,s)}^{n+1}) \right) \quad (s \in \partial D_d \setminus \partial\Omega).
 \end{aligned}$$

Introduce the following assumptions:

(H1)' (i) There are positive constants $\kappa_1, \kappa_2, \lambda_1, \lambda_2$ such that

$$\kappa_1 \leq \kappa(x, t) \leq \kappa_2, \quad \lambda_1 \leq \lambda(x, t) \leq \lambda_2, \quad \forall (x, t) \in \bar{\Omega} \times [0, T];$$

(ii) $\kappa(x, t), \lambda(x, t), f(x, t), g(x, t)$ are continuous on $\bar{\Omega} \times [0, T]$, and $\varphi(x, t)$ is continuous on $\bar{\Omega}$;

(iii) The problem (40)–(42) has a unique solution $u = u(x, t) \in C^{2,1}(\bar{\Omega} \times [0, T])$.

(H3)' $(\bar{\kappa}_{ps} + \bar{\kappa}_{ds})^2 \sin^2 \theta_s \leq 4\bar{\kappa}_{ps}\bar{\kappa}_{ds}$.

In the following $C = C(\varepsilon)$ is a positive constant dependent only on the known data and ε , which maybe different from line to line. And let

$$\|e^{n+1}\|_2^2 = \sum_{p \in \Omega} (e_p^{n+1})^2 \|P_p\| + \sum_d (e_d^{n+1})^2 \|D_d\|.$$

Using the similar methods of proof in Section 3, and the Gronwall inequality, we can get the following convergent theorem.

Theorem 2. Assume that the conditions **(H1)'**, **(H2)** and **(H3)'** are satisfied. Then, (i) the following estimate is satisfied.

$$\|e^{n+1}\|_2 \leq C(h + \Delta t);$$

(ii) there holds

$$\|e^{n+1}\|_2^2 + \sum_{k=0}^n \left(\|\nabla e^{k+1}\|_2^2 + \|\bar{\nabla} e^{k+1}\|_2^2 + \sum_{p \in \partial\Omega} \lambda_p^{k+1} (e_p^{k+1})^2 |S_{ps} \cap \partial\Omega| + \sum_{d \in \partial\Omega} \lambda_d^{k+1} (e_d^{k+1})^2 |D_d \cap \partial\Omega| \right) \Delta t \leq C(h + \Delta t)^2.$$

6. Numerical results

In [2] some interesting numerical results for both linear and nonlinear parabolic equations are given to show the second-order accuracy and the efficiency of the method. In this section we present the numerical results obtained on different meshes for several test problems. Four different types of meshes are used. One is a uniform mesh for the domain $\Omega = [0, 1] \times [0, 1]$. The number of cell center unknowns in the x and y directions are I and J respectively, and therefore the total number of mesh points is $(I + 1) \times (J + 1)$. The other three are distorted meshes. The first distorted mesh is a mesh with a sine domain (see Fig. 7) defined as $\Omega = \{(x, y) | 0 \leq x \leq 1, 0 \leq y \leq Y(x)\}$, where $Y(x) = 1 + \sin(2\pi x)/2$. The mesh is defined as

$$x_{ij} = \frac{i}{I}, \quad y_{ij} = \frac{jY(x_{ij})}{J}, \quad i = 0, 1, \dots, I, \quad j = 0, 1, \dots, J.$$

The second distorted mesh is a Z-mesh as described in [5], and it is shown in Fig. 5. The third distorted mesh is a random mesh. The random mesh over the physical domain $\Omega = [0, 1] \times [0, 1]$ is defined by

$$x_{ij} = \frac{i}{I} + \frac{\sigma}{I}(R_x - 0.5), \quad y_{ij} = \frac{j}{J} + \frac{\sigma}{J}(R_y - 0.5),$$

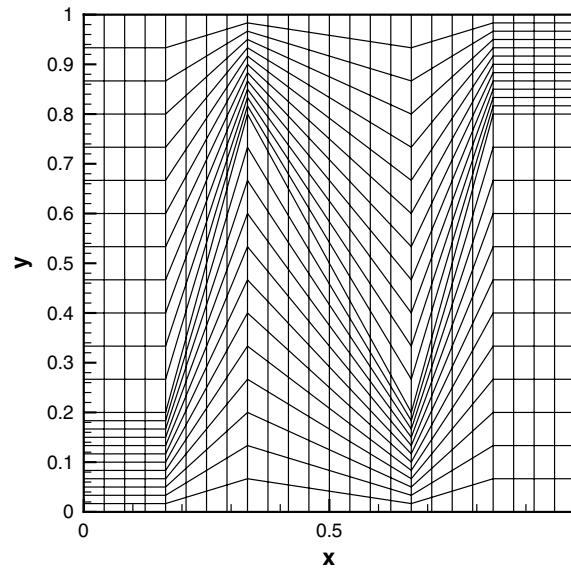
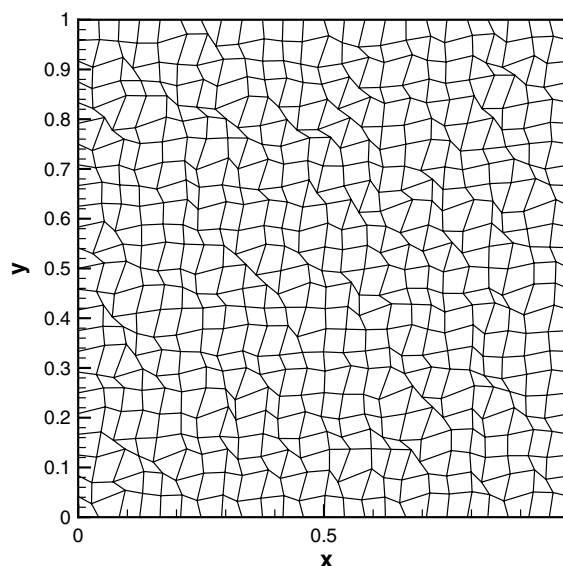


Fig. 5. Z-mesh.

where $\sigma \in [0, 1]$ is a parameter and R_x and R_y are two normalized random variables. When $\sigma = 0$ the mesh is uniform, and when σ is close to one it can become highly skewed. Fig. 6 is a random mesh generated with $\sigma = 0.7$.

Note that the linear system is symmetric and positive definite when $\bar{\kappa}_{ps} = \bar{\kappa}_{ds}(\forall s)$, and no more symmetric when $\bar{\kappa}_{ps} \neq \bar{\kappa}_{ds}$. In the following, the symmetric and positive definite linear systems are solved by the conjugate gradient method and the non-symmetric linear systems are solved by the biconjugate gradient stabilized algorithm.

Fig. 6. Random mesh ($\sigma = 0.7$).

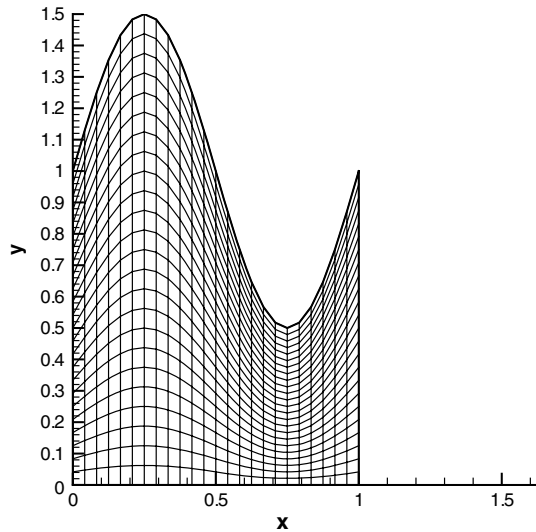


Fig. 7. Sin-mesh.

6.1. Linear elliptic equation

Consider the following linear elliptic equation whose exact solution is $u = 2 + \cos(\pi x) + \sin(\pi y)$:

$$\begin{aligned}
 -\nabla \cdot (\nabla u) &= \pi^2(\cos(\pi x) + \sin(\pi y)) \quad \text{in } \Omega, \\
 u &= 2 + \cos(\pi x) + \sin(\pi y) \quad \text{on } \partial\Omega_S \cup \partial\Omega_N, \\
 \nabla u \cdot \nu &= 0 \quad \text{on } \partial\Omega_E \cup \partial\Omega_W.
 \end{aligned}$$

In order to illustrate the robust of the method, we will give in Table 1 the error (maximum error) and the gradient of the error (H1-norm, see Theorem 1) between the exact solution and the computed solution for the four meshes: uniform mesh, sin-mesh, Z-mesh and random mesh. From this table, we can see that the method is almost second-order convergent for the maximum error on the four meshes, and the convergent order for

Table 1
Results for the linear elliptic equation

$I \times J$		12×12	24×24	48×48	96×96	192×192
Uniform mesh	Maximum error	1.08E-2	2.71E-3	6.77E-4	1.71E-4	4.54E-5
	Ratio	–	3.99	4.00	3.96	3.77
	H1-norm	6.31E-2	1.97E-2	6.39E-3	2.13E-3	7.26E-4
	Ratio	–	3.20	3.08	3.00	2.93
Sin-mesh	Maximum error	4.24E-2	1.05E-2	2.69E-3	6.78E-4	1.71E-4
	Ratio	–	4.04	3.90	3.97	3.96
	H1-norm	2.06E-1	6.39E-2	1.98E-2	6.33E-3	2.08E-3
	Ratio	–	3.22	3.23	3.13	3.04
Z-mesh	Maximum error	4.75E-2	1.27E-2	3.17E-3	8.02E-4	1.99E-4
	Ratio	–	3.74	4.01	3.95	4.03
	H1-norm	3.36E-1	1.11E-1	3.59E-2	1.17E-2	3.90E-3
	Ratio	–	3.03	3.09	3.07	3.00
Random mesh	Maximum error	1.67E-2	4.28E-3	1.25E-3	3.42E-4	9.31E-5
	Ratio	–	3.90	3.42	3.65	3.67
	H1-norm	1.24E-1	5.28E-2	2.51E-2	1.24E-2	6.12E-3
	Ratio	–	2.35	2.10	2.02	2.03

the gradient of the error is higher than 1.5 on the three first meshes and over 1 on the random mesh, which verify the theoretical results.

Then, we consider the general model diffusion problem

$$-\nabla \cdot (\kappa \cdot \nabla u) = f \quad \text{in } \Omega,$$

$$u = \sin(\pi x) \sin(\pi y) \quad \text{on } \partial\Omega.$$

Here κ is a symmetric positive definite matrix, $\kappa = RDR^T$, and

$$R = \begin{pmatrix} \cos \theta & -\sin \theta \\ \sin \theta & \cos \theta \end{pmatrix}, \quad D = \begin{pmatrix} d_1 & 0 \\ 0 & d_2 \end{pmatrix}$$

and

$$\theta = \frac{5\pi}{12}, \quad d_1 = 1 + 2x^2 + y^2, \quad d_2 = 1 + x^2 + 2y^2.$$

The solution is chosen to be

$$u(x, y) = \sin(\pi x) \sin(\pi y).$$

We present the numerical results obtained with the finite volume method (FVM) in the Section 2 and the support operators method (SOM) given by Shashkov in [11]. We use the program for support operators method attached to his book. The results on different meshes for FVM and SOM are presented in Tables 2 and 3, respectively.

Table 2
Results of FVM for the general model diffusion problem

	$I \times J$	12×12	24×24	48×48	96×96	192×192
Sin-mesh	Maximum error	2.05E-2	7.47E-3	2.36E-3	6.67E-4	1.79E-4
	Ratio	–	2.74	3.17	3.54	3.73
	H1-norm	1.95E-1	6.52E-2	2.11E-2	6.92E-3	2.30E-3
	Ratio	–	2.99	3.09	3.05	3.01
Z-mesh	Maximum error	5.80E-2	1.61E-2	3.89E-3	9.96E-4	2.50E-4
	Ratio	–	3.60	4.14	3.91	3.98
	H1-norm	4.55E-1	1.42E-1	4.30E-2	1.32E-2	4.21E-3
	Ratio	–	3.20	3.30	3.26	3.14
Random mesh	Maximum error	1.30E-2	3.24E-3	9.31E-4	2.48E-4	7.36E-5
	Ratio	–	4.01	3.48	3.75	3.37
	H1-norm	1.04E-1	5.37E-2	2.48E-2	1.27E-2	6.33E-3
	Ratio	–	1.94	2.17	1.95	2.01

Table 3
Results of SOM for the general model diffusion problem

	$I \times J$	12×12	24×24	48×48	96×96	192×192
Sin-mesh	Maximum error	2.66E-2	7.16E-3	1.83E-3	4.59E-4	1.15E-4
	Ratio	–	3.72	3.91	3.99	3.99
	H1-norm	1.02E-1	2.78E-2	7.24E-3	1.90E-3	5.13E-4
	Ratio	–	3.67	3.84	3.81	3.70
Z-mesh	Maximum error	3.93E-2	1.51E-2	4.95E-3	1.47E-3	4.52E-4
	Ratio	–	2.60	3.05	3.37	3.25
	H1-norm	3.17E-1	1.48E-1	5.69E-2	2.11E-2	7.63E-3
	Ratio	–	2.14	2.60	2.70	2.77
Random mesh	Maximum error	7.60E-2	2.65E-2	1.69E-2	1.35E-2	1.14E-2
	Ratio	–	2.87	1.57	1.25	1.18
	H1-norm	0.41	0.38	0.35	0.37	0.38
	Ratio	–	1.08	1.09	0.95	0.97

From Tables 2 and 3, we can see that (i) on the sin-mesh the accuracy of SOM is slightly higher than the accuracy of the FVM; (ii) on the Z-mesh, the SOM produces the better results than the FVM when the mesh is coarse, but the FVM produces the better results than the SOM when the mesh is refined enough; (iii) on the random mesh, the FVM produces significantly better results than the SOM. From these results it can be concluded that the finite volume method obtains the better results than the support operators method on Z-mesh and random mesh for this test problem.

The SOM often leads to a symmetric and positive definite coefficient matrix, however, it does not offer an explicit expression of discrete flux. The FVM used in this sub-section offers an explicit expression of discrete flux, however, it generally leads to a non-symmetric coefficient matrix, though the coefficient matrix is generally positive definite. The relation between these methods will be studied in future.

6.2. Linear elliptic equation with discontinuous coefficient

Consider the following linear elliptic equation with discontinuous coefficient,

$$-\nabla \cdot (\kappa(x, y) \cdot \nabla u) = f(x, y) \quad \text{in } \Omega,$$

where

$$\kappa(x, y) = \begin{cases} 4, & (x, y) \in (0, \frac{2}{3}] \times (0, 1), \\ 1, & (x, y) \in (\frac{2}{3}, 1) \times (0, 1) \end{cases}$$

and

$$f(x, y) = \begin{cases} 20\pi^2 \sin \pi x \sin 2\pi y, & (x, y, t) \in (0, \frac{2}{3}] \times (0, 1), \\ 20\pi^2 \sin 4\pi x \sin 2\pi y, & (x, y, t) \in (\frac{2}{3}, 1) \times (0, 1). \end{cases}$$

The exact solution of the problem is

$$u(x, y, t) = \begin{cases} \sin \pi x \sin 2\pi y, & (x, y, t) \in (0, \frac{2}{3}] \times (0, 1), \\ \sin 4\pi x \sin 2\pi y, & (x, y, t) \in (\frac{2}{3}, 1) \times (0, 1) \end{cases}$$

and the Dirichlet boundary condition is used.

Since κ is discontinuous across $x = 2/3$, we use the randomly distorted mesh shown in Fig. 8. Hence each primary element is homogeneous, but material properties vary across $x = 2/3$. In Table 4, we show the error

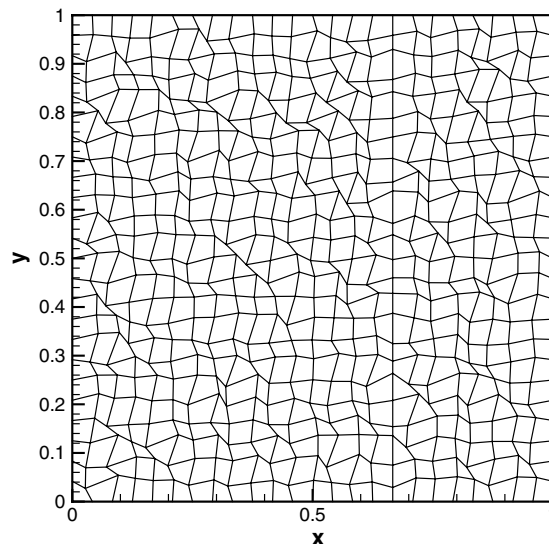


Fig. 8. Random mesh with a discontinuity in $x = 2/3$ ($\sigma = 0.7$).

Table 4
Results for the linear elliptic equation with discontinuous coefficient

	$I \times J$	12×12	24×24	48×48	96×96	192×192
Uniform mesh	Maximum error	7.66E-2	2.36E-2	6.50E-3	1.69E-3	4.31E-4
	Ratio	–	3.25	3.63	3.85	3.92
	H1-norm	7.03E-1	2.01E-1	5.90E-2	1.80E-2	5.70E-3
	Ratio	–	3.50	3.41	3.28	3.16
Sin-mesh	Maximum error	1.93E-1	5.93E-2	1.61E-2	5.00E-3	1.39E-3
	Ratio	–	3.25	3.68	3.22	3.60
	H1-norm	1.86	5.84E-1	1.69E-1	5.06E-2	1.58E-2
	Ratio	–	3.18	3.46	3.34	3.20
Z-mesh	Maximum error	6.44E-1	1.36E-1	3.93E-2	1.81E-2	9.96E-3
	Ratio	–	4.74	3.46	2.17	1.82
	H1-norm	4.74	1.42	3.86E-1	1.24E-1	5.10E-2
	Ratio	–	3.34	3.68	3.11	2.43
Random mesh	Maximum error	1.81E-1	3.53E-2	1.12E-2	3.13E-3	8.63E-4
	Ratio	–	5.13	3.15	3.58	3.63
	H1-norm	1.24	4.20E-1	1.66E-1	7.86E-2	3.82E-2
	Ratio	–	2.95	2.53	2.11	2.06

and the gradient of the error between the exact solution and the numerical solution for the four meshes: uniform mesh, sin-mesh, Z-mesh and random mesh with a discontinuity. From this table, we can see that the convergent order for the maximum error and the gradient of the error are higher than first-order on the four meshes.

6.3. Linear parabolic equation

Consider the following linear parabolic equation whose exact solution is $u = e^{-\pi^2 t}(2 + \cos(\pi x) + \sin(\pi y))$:

$$u_t - \nabla \cdot (\nabla u) = -2\pi^2 e^{-\pi^2 t} \quad \text{in } \Omega,$$

$$u = e^{-\pi^2 t}(2 + \cos(\pi x) + \sin(\pi y)) \quad \text{on } \partial\Omega_S \cup \partial\Omega_N,$$

$$\nabla u \cdot \nu = 0 \quad \text{on } \partial\Omega_E \cup \partial\Omega_W.$$

Table 5
Results for the linear parabolic equation ($\Delta t = 1.0E-5$, $T = 0.01$)

	$I \times J$	12×12	24×24	48×48	96×96
Uniform mesh	Maximum error	8.55E-3	2.14E-3	5.36E-4	1.36E-4
	Ratio	–	4.00	3.99	3.94
	H1-norm	4.53E-2	1.54E-2	5.35E-3	1.86E-3
	Ratio	–	2.94	2.88	2.88
Sin-mesh	Maximum error	4.08E-2	1.01E-2	2.60E-3	6.56E-4
	Ratio	–	4.04	3.88	3.96
	H1-norm	1.68E-1	5.43E-2	1.72E-2	5.61E-3
	Ratio	–	3.09	3.16	3.07
Z-mesh	Maximum error	2.76E-2	8.72E-3	2.34E-3	6.02E-4
	Ratio	–	3.16	3.73	3.89
	H1-norm	2.40E-1	9.00E-2	3.08E-2	1.05E-2
	Ratio	–	2.67	2.92	2.93
Random mesh	Maximum error	1.47E-2	3.61E-3	1.00E-3	2.45E-4
	Ratio	–	4.07	3.61	4.08
	H1-norm	1.06E-1	4.97E-2	2.46E-2	1.23E-2
	Ratio	–	2.13	2.02	2.00

In this computation, the time step size is chosen as $\Delta t = 1.0E-5$. With this small time step size, the time discretization error in our results can be ignored compared to the error from spatial discretization. We also give the error on four different meshes in Table 5. From this table, we can see that the method also recover second-order convergence for the maximum error and more than first-order convergence for the gradient of the error.

Next we discuss a problem whose solution has a large gradient. Consider the following linear parabolic equation:

$$u_t - \nabla \cdot (\kappa \nabla u) = f(x, y, t) \quad \text{in } \Omega.$$

The exact solution is $u = he^{-at} \arctan(b(ct - (x^2 + y^2))) + d$. Let $\kappa = Z$ and a, b, c, d, h, Z be the given constants. Moreover the boundary condition is taken as Dirichlet condition. We can see that the solution u has a large gradient at $x^2 + y^2 = ct$. We take $a = 0.01, b = 10, c = 1, d = 10, h = 1, Z = 1$. The computational domain is a sector, we use the regular mesh (Fig. 9) and random mesh (Fig. 10).

In Table 6, we give the maximum error and the gradient of the error for the regular mesh and random mesh respectively. From this table, we can see that the method also obtain the second-order convergence for the maximum error and more than first-order convergence for the gradient of the error.

6.4. Nonlinear parabolic equation

Consider the following nonlinear parabolic equation whose exact solution is $u = e^{-\pi^2 t}(2 + \cos(\pi x) + \sin(\pi y))$:

$$\begin{aligned} u_t - \nabla \cdot (\kappa(u) \nabla u) &= f(x, y, t) \quad \text{in } \Omega, \\ u &= e^{-\pi^2 t}(2 + \cos(\pi x) + \sin(\pi y)) \quad \text{on } \partial\Omega_S \cup \partial\Omega_N, \\ \nabla u \cdot \nu &= 0 \quad \text{on } \partial\Omega_E \cup \partial\Omega_W, \end{aligned}$$

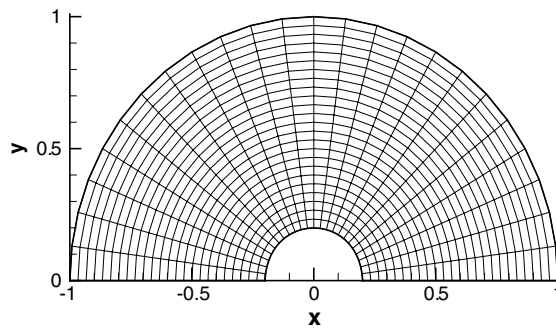


Fig. 9. Regular mesh.

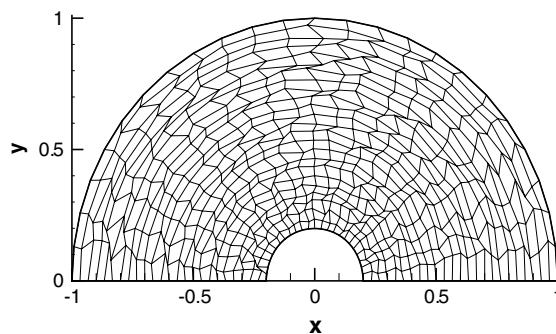


Fig. 10. Random mesh ($\sigma = 0.7$).

Table 6
Results for linear parabolic equation ($\Delta t = 1.0E-3$, $T = 0.4$)

	$I \times J$	12×12	24×24	48×48	96×96
Regular mesh	Maximum error	7.15E-2	1.59E-2	4.07E-3	1.01E-3
	Ratio	–	4.50	3.91	4.03
	H1-norm	6.30E-1	1.48E-1	3.68E-2	8.75E-3
	Ratio	–	4.26	4.02	4.21
Random mesh	Maximum error	3.32E-1	4.90E-2	8.97E-3	2.36E-3
	Ratio	–	6.78	5.46	3.80
	H1-norm	1.41	0.41	1.46E-1	6.30E-2
	Ratio	–	3.44	2.81	2.32

Table 7
Results for the nonlinear parabolic equation ($\Delta t = 1.0E-5$, $T = 0.01$)

	$I \times J$	12×12	24×24	48×48	96×96
Uniform mesh	Maximum error	8.46E-3	2.11E-3	5.32E-4	1.33E-4
	Ratio	–	4.01	3.97	4.00
	H1-norm	4.31E-2	1.48E-2	5.16E-3	1.82E-3
	Ratio	–	2.91	2.87	2.84
Sin-mesh	Maximum error	1.02E-1	2.31E-2	5.68E-3	1.43E-3
	Ratio	–	4.42	4.07	3.97
	H1-norm	3.29E-1	9.44E-2	2.93E-2	1.03E-2
	Ratio	–	3.49	3.22	2.84
Z-mesh	Maximum error	4.24E-2	1.28E-2	3.13E-3	7.83E-4
	Ratio	–	3.31	4.09	4.00
	H1-norm	3.89E-1	1.35E-1	4.26E-2	1.36E-2
	Ratio	–	2.88	3.17	3.13
Random mesh	Maximum error	1.06E-2	3.57E-3	9.04E-4	2.37E-4
	Ratio	–	2.97	3.95	3.81
	H1-norm	1.08E-1	5.31E-2	2.48E-2	1.24E-2
	Ratio	–	2.03	2.14	2.00

where $\kappa(u) = u$, $f = -\pi^2 e^{-\pi^2 t} (2 + \cos(\pi x) \cos(\pi y)) - \pi^2 e^{-2\pi^2 t} (\sin^2(\pi x) \cos^2(\pi y) + \cos^2(\pi x) \sin^2(\pi y)) + 2\pi^2 e^{-2\pi^2 t} (2 + \cos(\pi x) \cos(\pi y)) \cos(\pi x) \cos(\pi y)$. We give the errors for the four different meshes in Table 7. From this table, we can also obtain the similar results with those of the above subsection for the linear parabolic equation.

7. Conclusions and extensions

In this paper the truncation error of the discrete flux across the cell-sides is derived, and then the corresponding convergence theorem has been obtained, i.e., this method is of first-order convergence on highly distorted meshes. Moreover, the corresponding schemes for the diffusion equation with discontinuous coefficient and the non-stationary diffusion equation are also obtained. Numerical results are presented to demonstrate the performance of these schemes, which show that the method obtains nearly second-order convergence for the maximum error and more than first order convergence for the gradient of the error on highly distorted meshes.

There are some other locally conservative discretization methods, such as SOM and MPFA. Although the method in this literature and MPFA all have a nine-point stencil, the approaches of constructing discrete schemes are different. The relationship between the method in this paper and MPFA (or SOM) constitutes the subject of ongoing work.

To avoid that the dual elements contain different materials for the problem with discontinuous coefficient and decrease the computational cost, a simple method of weighted interpolation is proposed in [6], i.e., the unknown at the nodes of the primary mesh is expressed as the linear combination of the unknown at the center of neighboring primary elements. The reasonable choice of the weighted parameters is an important issue and is being studied now.

Acknowledgments

We thank Professor Tao Tang, Xudeng Hang and the two reviewers for their numerous constructive comments and suggestions that helped improving the paper significantly.

References

- [1] M. Berndt, K. Lipnikov, M. Shashkov, M.F. Wheeler, I. Yotov, Superconvergence of the velocity in mimetic finite difference methods on quadrilaterals, *SIAM J. Numer. Anal.* 43 (2005) 1728.
- [2] F. Hermeline, A finite volume method for the approximation of diffusion operators on distorted meshes, *J. Comput. Phys.* 160 (2000) 481.
- [3] Weizhang Huang, Practical aspects of formulation and solution of moving mesh partial differential equations, *J. Comput. Phys.* 171 (2001) 753.
- [4] Weizhang Huang, Andrew M. Kappen, A study of cell-center finite volume methods for diffusion equations, Mathematics Research Report, 98-10-01, University of Kansas, Lawrence KS66045.
- [5] D.S. Kershaw, Differencing of the diffusion equation in Lagrangian hydrodynamic codes, *J. Comput. Phys.* 39 (1981) 375.
- [6] Deyuan Li, Hongshou Shui, Minjun Tang, On the finite difference scheme of two-dimensional parabolic equation in a non-rectangular mesh, *J. Numer. Methods Comput. Appl.* 4 (1980) 217.
- [7] R. Li, T. Tang, P.W. Zhang, Moving mesh methods in multiple dimensions based on harmonic maps, *J. Comput. Phys.* 170 (2001) 562.
- [8] R. Li, T. Tang, P.W. Zhang, A moving mesh finite element algorithm for singular problems in two and three space dimensions, *J. Comput. Phys.* 177 (2002) 365.
- [9] K. Lipnikov, M. Shashkov, D. Svyatskiy, The mimetic finite difference discretization of diffusion problem on unstructured polyhedral meshes, *J. Comput. Phys.* 211 (2006) 473.
- [10] J.E. Morel, J.E. Dendy, M.L. Hall, S.W. White, A cell centered Lagrangian-mesh diffusion differencing scheme, *J. Comput. Phys.* 103 (1992) 286.
- [11] M. Shashkov, *Conservative Finite-difference Methods on General Grids*, CRC Press, Boca Raton, FL, 1996.
- [12] M. Shashkov, S. Steinberg, Support-operator finite-difference algorithms for general elliptic problems, *J. Comput. Phys.* 118 (1995) 131.
- [13] M. Shashkov, S. Steinberg, Solving diffusion equations with rough coefficients in rough grid, *J. Comput. Phys.* 129 (1996) 383.
- [14] J. Hyman, M. Shashkov, S. Steinberg, The numerical solution of diffusion problems in strongly heterogeneous non-isotropic material, *J. Comput. Phys.* 132 (1997) 130.
- [15] I. Aavatsmark, An introduction to multipoint flux approximations for quadrilateral grids, *Comput. Geosci.* 6 (2002) 405.
- [16] I. Aavatsmark, G.T. Eigestad, Numerical convergence of the MPFA O-method and U-method for general quadrilateral grids, *Int. J. Numer. Methods Fluids* 51 (2006) 939.
- [17] R.A. Klausen, T.F. Russell, Relationships among some locally conservative discretization methods which handle discontinuous coefficients, *Comput. Geosci.* 8 (2004) 341.
- [18] Donghyun You, Rajat Mittal, Meng Wang, Parviz Moin, Analysis of stability and accuracy of finite-difference schemes on a skewed mesh, *J. Comput. Phys.* 213 (2006) 184.
- [19] A. Winslow, Numerical solution of the quasi-linear Poisson equation, *J. Comput. Phys.* 1 (1967) 149.